Magnetic hyperthermia efficiency and MRI contrast sensitivity of colloidal soft/hard ferrite nanoclusters

Kosmas Vamvakidis,[a] Stefanos Mourdikoudis[b], Antonis Makridis[c], Eleni Paulidou,[c] Mavroeidis Angelakeris[c] and Catherine Dendrinou-Samara[a*]

[a]Department of Chemistry, Aristotle University of Thessaloniki, 54124 Thessaloniki, Greece;

[b]Departamento de Quimica Fisica, Universidade de Vigo, 36310 Vigo, Spain

[c]Department of Physics, Aristotle University of Thessaloniki, 54124 Thessaloniki, Greece

Corresponding Author

[*]e-mail: samkat@chem.auth.gr

ABSTRACT

The use of magnetic nanostructures as theranostic agents is a multiplex task as physiochemical and biochemical properties including excellent magneto-responsive properties, low toxicity, colloidal stability and facile surface engineering capability are all required. Nonetheless, much progress has been made in recent years synthesis of "all-in-one" MNPs remain unambiguously challenging. Towards this direction, in this study is presented a facile incorporation of a soft magnetic phase ($MnFe_2O_4$ NPs) with a hard phase ($CoFe_2O_4$ NPs) in the presence of the biocompatible polymer sodium dodecyl sulfate (SDS), into spherical and compact bi-magnetic nanoclusters (NCs) with modulated magnetic properties that critically enhance hyperthermic efficiency and MRI contrast effect. Hydrophobic $MnFe_2O_4$ and $CoFe_2O_4$ NPs coated with oleylamine of the same size (9nm) were used as primary building units for the formation of the bi-magnetic NCs through a microemulsion approach where a set of experiments were conducted to identify the optimal concentration of SDS (19.5 mM) for the cluster formation. Additionally, homo-magnetic NCs of $MnFe_2O_4$ NPs and $CoFe_2O_4$ NPs, respectively were synthesized for comparative studies. The presence of distinct magnetic phases within the bi-magnetic NCs resulting in synergistic behavior, where the soft phase offers moderate coercivity H_c and the hard one high magnetization M_s. Increased specific loss power (SLP) value was obtained for the bi-magnetic system (525 W/g) when compared with the homo-magnetic NCs (104W/g for MnNCs and 223W/g for CoNCs) under field conditions of 25 kA/m and 765 kHz. Relaxivities (r_2) of the bi-magnetic NCs were also higher (81.8 $mM^{-1}s^{-1}$) than those of the homo-magnetic NCs (47.4 $mM^{-1}s^{-1}$ for MnNCs and 3.1 $mM^{-1}s^{-1}$ for CoNCs), while the high r_2/r_1 value renders the system suitable for T_2-weighted MRI imaging.

KEYWORDS: magnetic nanoclusters, bi-magnetic systems, microemulsions, contrast agents, magnetic hyperthermia

1. Introduction

The well-established knowledge on the ability to tune the morphology and the physiochemical properties of individual nanoparticles (NPs) enables scientists to advance their research efforts in fabrication of more complex superstructures, such as nanoclusters (NCs) [1-4]. The formation of compact and spherical arrangements by clustering of primary NPs as building blocks, opens a new research area in materials science as improved or collective properties can be obtained by bringing nanocrystals next to one another and facilitate their use in diverse technological sectors [5,6]. Nanoclusters can be produced either through a number of different one-step techniques, including thermolysis [7], solvothermal [8] and microwave [9] methods or by multi-step processes such as microemulsions [10], electrostatic attraction [11], or interfacial tension [12]. Microemulsion-based approach has been the most attractive method to form such nanostructures as it presents the advantage of being more flexible for organizing nanoparticles of a large variety of materials [13]. Recently function-driven requirements led to the growth of multifunctional nanoclusters, consisting of two or more chemically different NPs that represent advanced nanoparticulate platforms [14-16]. For example, maximizing hysteresis losses in magnetic hyperthermia (MH), while achieving a high magnetization for effective contrast sensitivity in magnetic resonance imaging (MRI), that is highly desirable for theranostic purposes [17]. However, it is still challenging to enhance the magnetic properties of nanostructures in order to achieve higher signal sensitivity for better contrast in MRI and for improving the heating efficiency in MH.

One common way to control magnetic properties is the combination (in a different or the same volume ratios) of a soft with a hard magnetic phase, such as $MnFe_2O_4$ and $CoFe_2O_4$, in core-shell particles, multi-layers or thin films architectures [18-24]. By combining the high coercivity of the hard material with the high saturation magnetization of the soft material, it's possible to increase the maximum energy product of the nanocomposite, expressed as $(BH)_{max}$, when compared with the individual counterparts. These bi-magnetic systems always present exchange coupling at their interfaces, which is reflected to the shape of hysteresis loops [25,26]. Magnetization curves appear smooth behaving like a single magnetic phase material, without unusual drops or kinks, as the two phases reverse at the same field. However, the synthesis of core-shell structures remains a complex approach as the structural quality of the shell may be inferior and post-synthesis treatments are needed due to the non-homogeneous growth conditions [27]. The precise control of the thin film thickness is also a difficult task to be achieved [28]. Moreover, the characterization of these systems is quite demanding as advanced techniques are needed such as ΔM-plots, first order reversal curves (FORC), small angle neutron scattering (SANS), or element-specific X-ray magnetic circular dichroism (XMCD). Finally, to probe the effects of coupling such as positive exchange bias, compensation points or proximity effects, sophisticated Monte Carlo simulations should also be conducted. For these reasons a practical demand for the development of simpler nanocomposite bi-magnetic systems is imperative in order to satisfy specific application requirements.

Recently, we designed multi-responsive water-soluble graft copolymers that were used for the formation of bi-magnetic ferrite nanoclusters and were found to act simultaneously as luminescent, hyperthermia and contrast MRI agents [29]. However, concerning the complicate chemical process needed for the production of such

polymers, plus their low yield, in the present work we chose to use a commercial biocompatible polymer such as sodium dodecyl sulfate (SDS). In so, we propose for the first time a facile incorporation of a soft magnetic phase ($MnFe_2O_4$ NPs) with a hard phase ($CoFe_2O_4$ NPs) into spherical and compact bi-magnetic nanoclusters covered by SDS molecules. In these NCs the soft phase is not coupled with the hard phase, because the primary particles/building blocks were coated by oleylamine, which hinders the direct physical contact among them within each cluster. Hysteresis loops are no longer smooth and a constriction at low fields is observed. However, even though exchange coupling is not established, the bi-magnetic NCs present synergetic behavior where the properties of each counterpart are combined. To confirm the distinct magnetic characteristics of the bi-magnetic structure, we performed comparative studies with homo-magnetic NCs that consist of $MnFe_2O_4$ or $CoFe_2O_4$ NPs respectively. Our results clearly show that the magnetic properties of the bi-magnetic NCs are distinctively different from those of homo-magnetic NCs. Coercivity was finely tuned maximizing hysteretic losses, while high magnetization value was observed. In order to evaluate the performance of these NCs as a possible bifunctional targeting system, the heating efficiency was obtained by means of specific loss power (SLP) estimations while the relaxivities (r_1 and r_2) were also determined by clinical MRI studies.

2. Materials and methods

2.1. Materials

All the reagents were of analytical grade and were used without any further purification. The products necessary for our experiments are the following: Sodium

Dodecyl Sulfate, $CH_3(CH_2)_{11}SO_4Na$, (SDS) (Aldrich, ≥ 99%), Cyclohexane, C_6H_{12}, (Aldrich, ≥ 99.9%). Milli-Q water was used with a resistivity no less than 18.2 MΩ cm^1.

2.2. Synthesis of nanoclusters

Hydrophobic manganese and cobalt ferrite nanoparticles coated with oleylamine were synthesized following the solvothermal method published previously by our group [30,31]. For the synthesis of the bi-magnetic ferrite NCs (Mn@CoNCs) 7.5 mg of $MnFe_2O_4$ NPs and 7.5 mg of $CoFe_2O_4$ NPs were dissolved in cyclohexane (3 mL) and added dropwise to an aqueous solution (30 mL) of SDS (168 mg). The mixture was emulsified by sonication treatment and in the next step cyclohexane was evaporated at the desired temperature and for a specified time. Once cyclohexane evaporated water was added to keep the volume constant (30 mL). The as-prepared colloids were purified three times with ethanol, centrifuged at 5000 rpm for 20 min and finally the nanoclusters were re-dispersed into water. A small part was dried to obtain dry nanoclusters for further characterization. By using the above procedure, nanoclusters consisted only of $MnFe_2O_4$ NPs (15 mg) or $CoFe_2O_4$ NPs (15 mg) were also formed, hereafter named as MnNCs and CoNCs, respectively.

2.3. Characterization

Conventional TEM images were obtained with a JEOL 1010 microscope (TEM), operating at an acceleration voltage of 100 kV. For TEM observations we have used suspensions of the nanoparticles deposited onto carbon-coated copper TEM grids. The elemental composition of the samples was tested by scanning electron microscopy (SEM: JEOL 840A), where energy dispersive X-ray spectrometry (EDS) spectra were obtained. Fourier transform infrared spectroscopy (280-4000 cm^{-1}) was recorded using

a Nicolet FT-IR 6700 spectrometer with samples prepared as KBr pellets. Thermogravimetric analysis (TGA) was performed using SETA-RAM SetSys-1200 and carried out in the range from room temperature to 800 ^{0}C at a heating rate of 10 ^{0}C min^{-1} under N_2 atmosphere. Magnetic measurements were performed using a vibrating sample magnetometry (VSM) (P.A.R. 155). ζ-potentials were determined by electrophoretic measurements, carried out at 25 °C by means of a NanoZetasizer, while hydrodynamic diameters were recorded by Nano ZS Malvern apparatus (DLS). The incident light source was a 4 mW He–Ne laser at 633 nm and the intensity of the scattered light was measured at 173°. Heating experiments were performed in an arrangement using a water-cooled induction coil of 23 mm diameter consisting of three turns, producing an alternating magnetic field (AMF) with a frequency of 765 kHz and an amplitude of 300 Oe (25 kA m^{-1}). The ac field was generated by means of a commercial generator with a power of 4.5 kW. Temperature was monitored with a fiber optic probe placed in the center of the heated vial. During measurement, heating and natural cooling sequences were recorded, each of them, for about 600 s. SLP values were extracted from the initial slope of the heating curve before the interference of heat conduction becomes significant [32]. In order to extract a more accurate SLP value, the reference signal corresponding to the solvent was subtracted from the measured data, while the thermal losses to the environment were also considered in the SLP estimation [33]. The heating capacity of the superparticles was quantified by the specific loss power (SLP), defined as the amount of energy converted into heat per time and mass. The longitudinal (T_1) and transverse (T_2) relaxation times measurements at different concentrations (0.0125-0.8 mM) of the metal ions were performed on a clinical MRI Scanner (a 1.5 T Siemens Aera) using a Head/Neck coil. The T_1-weighted images were obtained by an inversion recovery (IR) T_1 pulse sequence with variable inversion values

(IR=25 - 4000 ms) and an echo time (T_E) of 12 ms (1.5 T)/43 ms (1.5 T). Imaging parameters were as follows: 1.5 T; field of view (FOV)=250.250 mm^2, matrix size (MTX)=128.128, number of axial slices=1, slice thickness=20 mm, and number of averages (NEX)=1. T_2-weighted images were obtained by a multi-echo spin-echo T_2 pulse sequence (5 echoes; 25-50-75-100-125 ms, and static TR (2000 ms). Imaging parameters were as follows: 1.5 T; FOV=250·250 mm^2, MTX=256·128, number of axial slices=1, slice thickness=5.0 mm, and NEX=1. The resulting set of images was processed off-line using an image sequence analysis tool developed in IDL (IDL 8.2, Bolder, USA). T_1 and T_2 analyses were carried out by fitting a monoexponential curve on the image intensities measured on the selected regions of interest (ROIs) for each axial slice.

3. Results and discussion

A simple microemulsion-based approach is applied for the synthesis of spherical and compact bi-magnetic ferrite nanoclusters combining for the first time a soft magnetic phase ($MnFe_2O_4$ NPs) with a hard phase ($CoFe_2O_4$ NPs) through the biocompatible sodium dodecyl sulfate (SDS) polymer. Emulsion droplets are convenient templates to confine particles into clusters by evaporating the dispersion solvent. The assembly was driven by the hydrophobic van der Waals interactions of the capping ligands (oleylamine) on the nanoparticle surface with the surfactant molecules (SDS), while the diameter of the colloidal clusters can be controlled by adjustment of the emulsification process [34]. To increase compactness of the final clusters, the self-assembly of NPs was typically followed by gentle solvent evaporation below 60˚C [34]. However, the specific position of nanoparticles in desired locations within clusters is not still feasible. We select as primary particles MNPs with the same morphology and

size (9 nm), in order to avoid great differences in their free Gibbs energy. The cobalt ferrite NPs displayed higher magnetization (85 emu/g) and coercivity (250 Oe) than the $MnFe_2O_4$ NPs (66 emu/g, 150 Oe) [30, 31]. The inversion degree of the manganese ferrite NPs was reduced due to synthetic conditions leading to an improved magnetic performance [30]. We chose to combine a phase with high M_s and H_c, with one of lower M_s and H_c in order to tailor coercivity close to the amplitude of the alternating magnetic field (AMF) which was used for the hyperthermia experiments (300 Oe). Moreover, both ferrite NPs were thoroughly coated with oleylamine, because imperfect surface functionalization often creates a non-uniform interparticle-interaction environment, leading to the formation of NCs with short-range order and sometimes loose structures [35].

3.1. Optimal SDS concentration

For the stabilization of the emulsion we used the anionic surfactant, sodium dodecyl sulfate (SDS), which possesses a hydrocarbon tail in combination with a polar headgroup, while micelles with amphiphilic properties created. In general, formation of micelles initiates above the critical micelle concentration (CMC) of surfactant, 8.2 mM for SDS [36]. However, as the stability and structure of microemulsions depends on the concentration of the polymer, a set of experiments were conducted to identify the optimal concentration of ligand protection for cluster formation [37]. Starting with a concentration slighter higher than the CMC (9 mM) we found that the organic molecules are not enough for the full surface coverage and in so not all the particles gathered within clusters but isolated NPs were also present (Fig. 1a). Same results were found at even higher concentration (12 mM) as shown in Fig. 1b. Increasing more the concentration of SDS (15 and 17.5 mM) the particles formed very loose clusters, which

are easily ruined during evaporation (Fig. 1c and d). Optimal concentration for clustering was found at about 19.5 mM, where sufficient surfactant molecules were present to saturate clusters' surfaces (Fig. 1e). Above this value (20 mM) nanoparticles together with nanoclusters were embedded into extended networks (Fig. 1f).

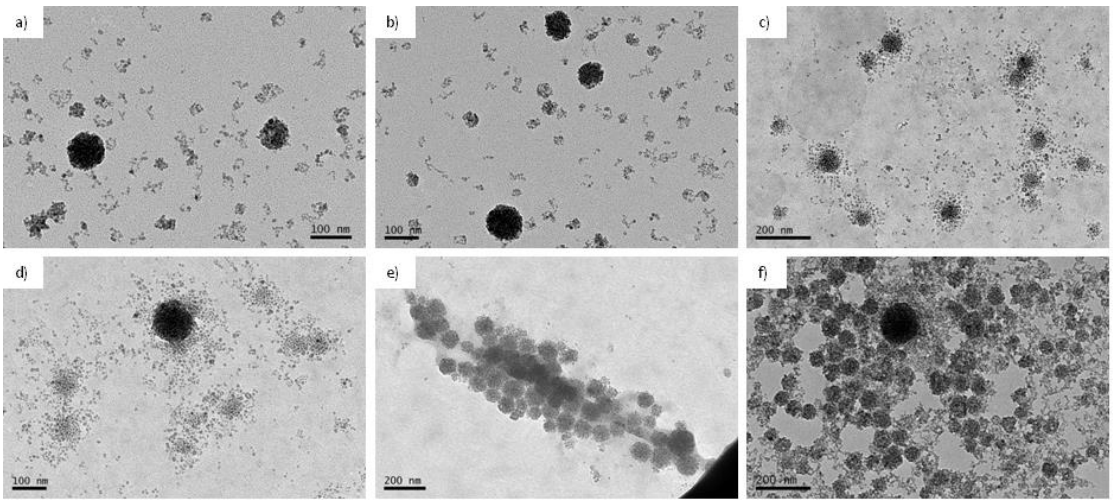

Fig. 1. TEM images of experimental variations in SDS concentration; (a) 9 mM, (b) 12 mM, (c) 15, (d) 17.5 mM, (e) 19.5 mM and (f) 20 mM.

3.2. Morphological and compositional characterization of the bi-magnetic nanoclusters

Fixing the SDS concentration at the above optimal value (19.5 mM) bi-magnetic ferrite NCs were synthesized (Mn@CoNCs). The size of the resulted compact NCs were 81 nm ±19 nm (Fig. S1a Supporting Information) as shown in the Fig. 1e, while these 3D colloidal spheres could self-assemble into ordered two-dimensional arrays on the TEM grid, which indicates that may serve as mesoscale building blocks for more complex macroscopic functional architectures. The successful formation of clusters was also verified by FT-IR spectroscopy. As shown in Fig. S2a (Supporting Information) the most intense peak of pure SDS at 1216 cm^{-1} is present at the spectra

of clusters shifted at 1188 cm^{-1}. The effective coating of the clusters is obvious also in TEM images (Fig. 2c). TGA results given in Fig. S2b (Supporting Information) revealed that the major weight loss of approximately 58 % for the clusters was contributed to the organic moieties, while in comparison with the organic amount of nanoparticles (~16 %) is found larger as expected. To confirm that the stable spherical assemblies exist in solution, we chose dynamic light scattering (DLS) to analyze these colloidal spheres. Their hydrodynamic diameters were found equal to 105 nm (Fig. 2b), close to the TEM results. In order to verify that both $MnFe_2O_4$ and $CoFe_2O_4$ nanoparticles have been successfully encapsulated together, multiple regions of the sample were analyzed by EDS elemental mapping during the SEM measurements. As shown in Fig. 2a EDS mapping justified the presence of all the three main elements in the Mn@CoNCs, namely Fe, Mn and Co as well as their homogeneous spatial distributions. Since nanoclusters are so ultrasmall, an elemental map image of each individual cluster could not be obtained. Therefore, we provided overall elemental map images of the sample. As expected, identical elemental map images for Mn and Co were observed, implying that nanoparticles are mixed homogeneously throughout all the volume of the cluster. Furthermore, the relative atomic abundance (%) of the different components (Mn, Co and Fe) obtained from the EDS spectra reveals similar concentrations of manganese (19.96%) and cobalt (20.06%) while iron was found (80.98%) in accordance with the generic formula of ferrites (MFe_2O_4, M=Mn, Co).

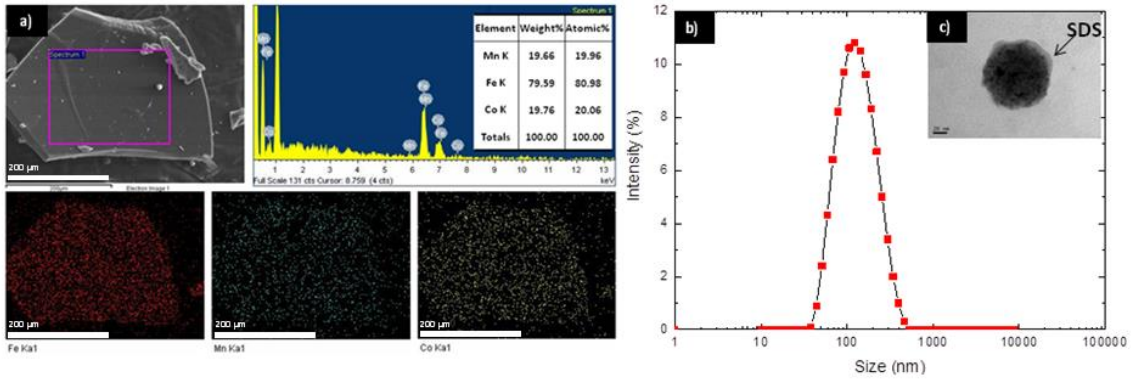

Fig. 2. (a) Indicative EDS elemental map images; (b) DLS measurements of aqueous suspensions of the NCs; (c) arrow indicates SDS coating on the surface of NCs.

For comparative studies two additional samples of NCs were synthesized using as building blocks solely $MnFe_2O_4$ NPs and $CoFe_2O_4$ NPs (sample named as MnNCs and CoNCs respectively). Their TEM images (Fig. 3a and b) revealed the formation of dense spherical nanoclusters without any free particles left out and mean size of 75 ± 23 nm and 95 ± 12 nm, respectively (Fig. S1b,c Supporting Information), while their hydrodynamic diameters obtained by DLS analysis were 80 nm and 110 nm (insets).

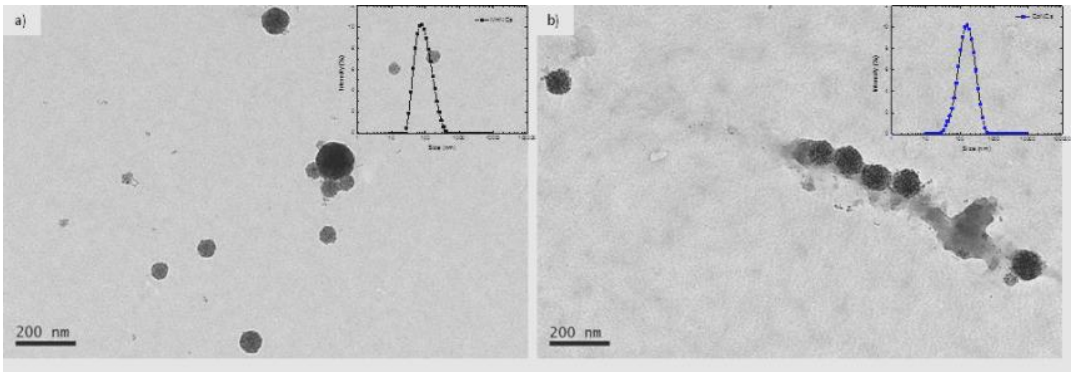

Fig. 3. TEM images and hydrodynamic diameters of (a) MnNCs and (b) CoNCs, respectively.

3.3. Static Magnetic properties

Room temperature hysteresis loops were recorded both in nanoparticles and nanoclusters in order to probe the magnetization improvement as well as the emerged variations in coercivity (Fig. 4a). The absolute values of magnetization (M_S) were estimated using the effective mass according to the weight loss that resulted from the TGA data. Considering that the average sizes and hydrodynamic diameters of the obtained NCs were similar, the differences in Ms and H_c can be correlated mainly with their composition. As shown in Table 1 magnetization values for both MnNCs and CoNCs were increased, with respect to the primary NPs, by approximately 30 % and 20 %, respectively. The assembly of magnetic NPs in secondary structures not only propels their magnetic moments to interact through various processes, but as expected an enhanced saturation magnetization compared to that of individual nanocrystals was shown [4]. Generally, this enhancement originates from dipole-dipole and exchange interactions. However, when adjacent particles are capped by a layer of long-chain organic ligands the distance among them prevents exchange interactions rendering dipole-dipole interactions dominant [38]. As dipolar interactions, which are long-range and anisotropic, become larger than thermal fluctuations they can result in ordering of the moments improving the effective M_s of clusters, as was observed [39]. It is interested to note that the Ms values were higher than the bulk values owing to the reduced inversion degree of the primary nanoparticles induced a change of the cation distribution within the spinel lattice [30]. In contrast, coercivity was affected by a different way upon clustering. The soft magnetic phase ($MnFe_2O_4$) retained the same coercive field either as single particles or spherical nanoclusters, while for the hard phase ($CoFe_2O_4$) coercivity was almost doubled in the case of nanoclusters. The higher coercivity of the $CoFe_2O_4$ NPs stems from the Co^{+2} cations within the spinel structure which contribute strongly to the cubic magneto-crystalline anisotropy because their

ground state retains some orbital degeneracy and is embedded in a crystal field of reduced symmetry.

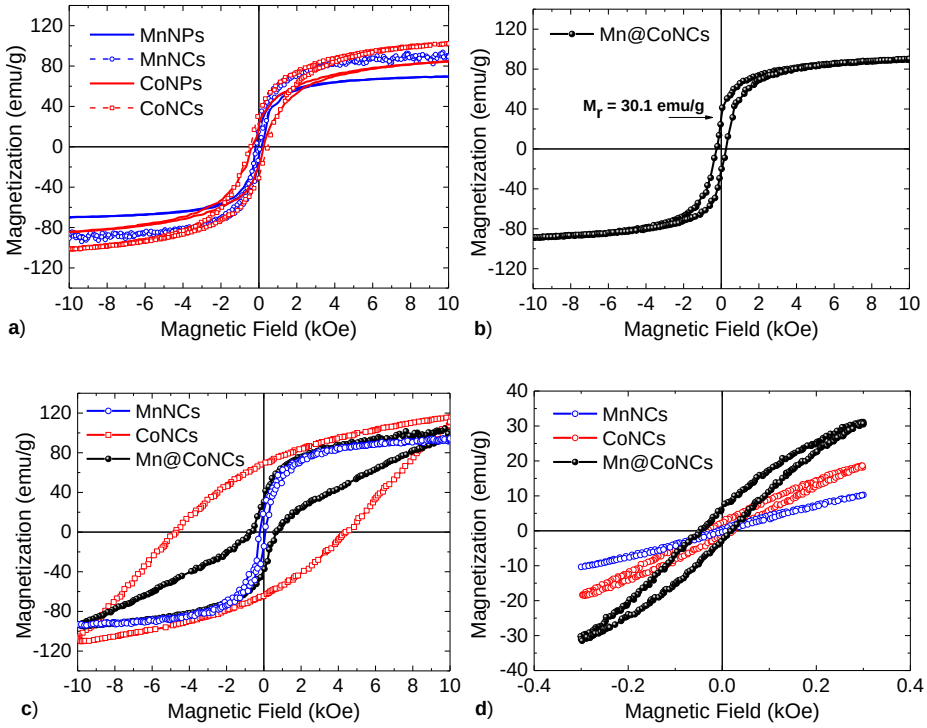

Fig. 4. (a) Nanoparticles versus nanoclusters, (b) Hysteresis loop of the Mn@CoNCs at 300 K, (c) Hysteresis loops of the three NCs samples measured at 80 K and (d) Minor loops of the NCs recorded at 300 K under field conditions of 25 kA/m and 765 kHz.

After the comparison between particles and clusters we measured the field dependent magnetization of the bi-magnetic Mn@CoNCs (Fig. 4b). This system showed the highest saturation moment of about 90 emu/g, with a moderate anisotropy of 250 Oe. Additionally, the remanent magnetization (M_r) of the nanocomposite is not larger than the half of the saturation magnetization ($M_r/M_s < 0.5$), which indicates the absence of exchange coupling between the two magnetic phases according to the Stoner-Wohlfarth theory [40]. To highlight if the two magnetic phases are coupled within each cluster, we carried out hysteresis cycles of the Mn@CoNCs at 80 K in water

to minimize dipole-dipole interactions between the clusters. The same measurement was obtained for the samples MnNCs and CoNCs for comparison reasons. As shown in Fig. 4c the MnNCs present quite lower coercivity (100 Oe) than the CoNCs (close to 4.5 kOe), while magnetizations was found equal to 88 emu/g and 116 emu/g, respectively. Saturation magnetization of all samples recorded by VSM has an absolute uncertainty of 6%, thus the larger Ms value of MnNCs at room temperature (88 emu/g) comparing with lower Ms value (93 emu/g) at 80 K is related to the precision limitations of the measurement device. For the bi-magnetic NCs we found also high M_s (97 emu/g) but coercivity was decreased (close to 700 Oe). However, the most interesting feature of the loop is the fact that is no longer smooth, presenting a shrinkage at lower fields. That means that the two phases do not reverse at the same nucleation field, as the soft phase nucleates the reversal at significantly lower fields and the switching is characterized by an inhomogeneous reversal [27, 34, 41]. The symmetric shape with respect of the origin demonstrates the absence of exchange bias, as the $MnFe_2O_4$ and $CoFe_2O_4$ nanoparticles are not in intimate contact within each cluster due to the layer of oleylamine on their surface. Therefore, exchange coupling between the two phases has not been established while coherent magnetization rotation is not observed. This observation confirms the presence of distinct magnetic phases within the NCs, resulting in synergistic behavior, where the soft phase ($MnFe_2O_4$) offers moderate coercivity H_c and the hard phase ($CoFe_2O_4$) high magnetization M_s. The overall magnetic behavior is a simple superposition of the properties of each phase. The loops that were recorded at 80 K clearly show that the two phases act magnetically independent in contrast with the loops at 300 K. This alteration stems from the different preparations that were followed before the measurement of each sample. At 80 K a frozen ferrofluid was formed where the rotation movement of the nanoclusters was hindered as they were in

fixed positions during the field increase. At this state the dipole-dipole interactions among the clusters were minimized and the signal was generated mostly from the interior of the clusters. The measurement of M_s at 300 K was recorded at a dry sample (powder) where the clusters were in close contact to each other and by this way the interactions among them were present and depicted to the smoothness of the hysteresis loop.

Table 1 Magnetic properties of the nanostrustures and their performance in MH and MRI.

Sample	300 K		80 K					
	M_s (emu/g)	**H_C (Oe)**	**M_s (emu/g)**	**H_C (Oe)**	**SLP (W/g)**	**r_1 ($mM^{-1}s^{-1}$)**	**r_2 ($mM^{-1}s^{-1}$)**	**r_2/r_1**
MnNPs	66	150	-	-	27	-	-	-
CoNPs	85	250	-	-	40	-	-	-
MnNCs	93	152	88	100	104	3.9	47.4	12.1
CoNCs	102	460	116	4500	223	0.2	3.1	14.8
Mn@CoNCs	90	250	97	700	525	5.2	81.8	15.8

3.4. Measurements of the Specific Loss Power

Time-dependent calorimetric measurements were performed both on nanoclusters and nanoparticles to compare their heating efficacy and detect the best heating agents. Generally, the heating capacity of a magnetic material is quantified by the specific loss power (SLP), defined as the amount of energy converted into heat per time and mass and calculated by the following relation:

$$SLP = C_P \frac{m_f}{m_{NPs}} \frac{\Delta T}{\Delta t}$$

where C_p is the specific heat of the solution, m_f is the sample volume, m_{NPs} is the mass of magnetic material in the sample and $\Delta T/\Delta t$ the initial slope of the heating curve. The heating curves of the samples together with the reference signal from the water are

shown in Fig. 5a. In all cases the measured volume of the aqueous dispersions was kept constant (1 mL), as well as the concentration of the magnetic material (1 mg/mL). Firstly, we observed a 4-and-6-fold increase for the nanoclusters with respect to single nanoparticles (Table 1). However, the best SLP was obtained for the bi-magnetic system Mn@CoNCs (525 W/g). Under field conditions of 25 kA/m and 765 kHz the temperature increased at a rate of 0.2 ˚C/s reaching 60 ˚C in 2.8 min.

The heat generated by magnetic fluids under an AMF is mainly attributed to contributions of hystersis loss and Néel–Brownian relaxation losses. However, the SLP value attributed to hysteresis losses is much larger than that originating from Brownian and Néel relaxations [18]. In case of nanoclusters we do not expect them to show Brownian or Néel effects, especially at high frequency as that one of 765 kHz used in our experiments. The appearance of the room temperature ferrimagnetism of the NCs indicates that the hysteresis losses might play a significant role in the heat generation. In so minor loops at room temperature under a field equal to hyperthermia field amplitude were recorded (Fig. 4c). The different shape of the minor loops compared to the loops recorded at 80 K is again attributed to the way that the measurements were done. In contrast with the frozen ferrofluid at 80 K, for the hyperthermia experiments the clusters were dispersed in water at 300 K where they were free to move and interact to each other resulted to the smoothness of the hysteresis loop. Besides that MnNCs presents the highest magnetic permeability and even though they present low coercive field value (~150 Oe), as shown in figure 4c, their soft magnetic hysteresis loop does not allow their magnetization to fully saturate at the external field of 300 Oe, instead, at this field a weak saturation magnetization value is just reached, close to 10 emu/g. On the other hand, Mn@CoNCs present a nearly square loop at the region of 300 Oe (see figure 4c) and this allows them to get the complete energy benefit also at a minor

magnetic loop at 300 Oe and present high Ms (over 30 emu/g). The results show that the bi-magnetic NCs show enhanced hysteresis losses due to the internal arrangement of the soft and hard phases leading to increased $(BH)_{max}$ product. For this sample we also recorded hyperthermia profiles as a function of concentration (0.25, 0.5, 1.0 and 2.0 mg/mL) (Fig. 5c,d). The SLP values of the bi-magnetic NCs is independent from concentration, while in comparison with magnetic nanoclusters that have been tested at similar experimental conditions, they present better heating capacity [42]. Clustering cobalt ferrite NPs led to nanoclusters with coercivity larger than 300 Oe preventing the fast reversal of magnetization. In contrast manganese ferrite nanoclusters showed lower Hc together with low Ms. Only the bi-magnetic nanoclusters presented coercivity similar to the hyperthermia set up. Although a relatively high frequency has been applied in the experiments, analogous protocols are currently examined as alternatives to overcome the usual constraints of limited heat efficacy [43,44].

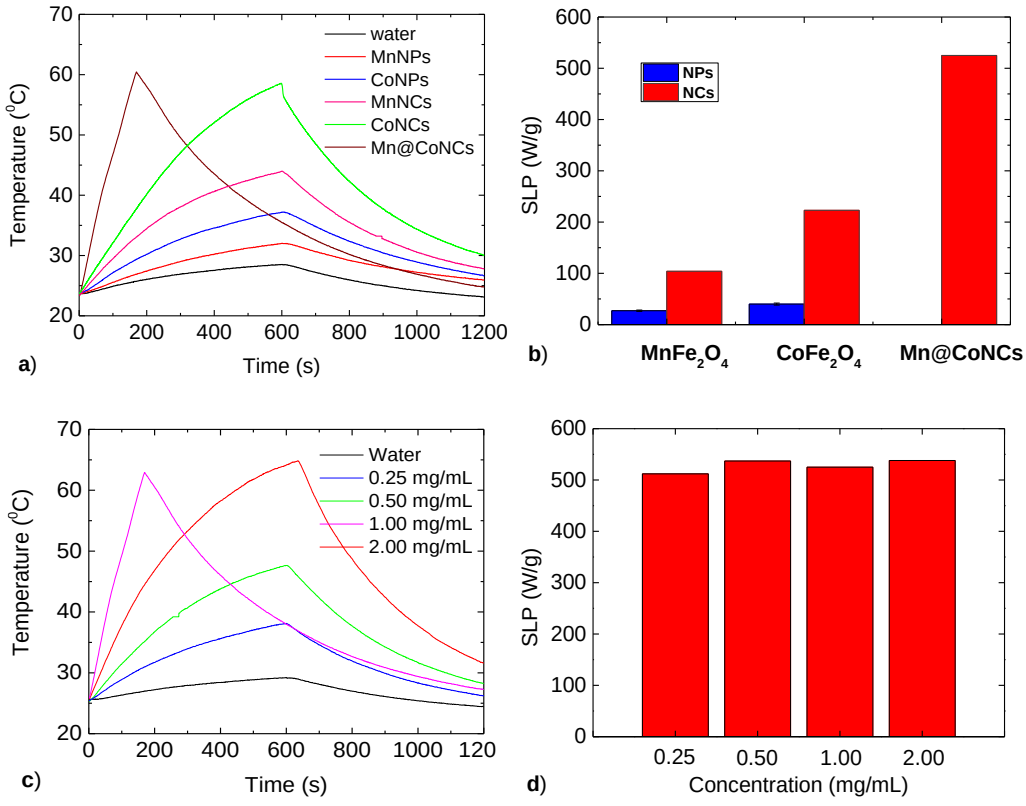

Fig. 5. (a) Heating curves of NPs and NCs, (b) SLP values of NPs and NCs, (c) Heating curves of the Mn@CoNCs in different concentrations and (d) SLP values of the Mn@CoNCs.

3.5. Preliminary MRI studies

MRI studies were performed in order to evaluate further application of the nanoclusters (MnNCs, CoNCs, Mn@CoNCs) as contrast agents. Under an external magnetic field, NCs generate local magnetic field inhomogeneities, which accelerate the dephasing rate of Larmor precession of surrounding water protons affecting the relaxation process [45]. There are two independent relaxation processes, i.e., longitudinal (T_1) and transverse (T_2) relaxation, which are typically used to generate the magnetic resonance images. The relaxation rate ($R=1/T_{1,2}$) increases linear with the NCs concentration according to the equation:

$$\frac{1}{T_{1,2}} = \frac{1}{T_0} + r_{1,2}C$$

where $1/T_{1,2}$ is the observed relaxation rate in the presence of the nanoparticles, $1/T_0$ the relaxation rate of pure water and C the concentration of NCs. Fig. 6a and b show the transverse relaxation rates (R_1 and R_2) for various metal concentrations of the NCs. It is clear that the $r_{2,1}$ relaxivities of the bi-magnetic Mn@CoNCs are higher (81.8/5.2 $mM^{-1}s^{-1}$) than those of the MnNCs and CoNCs) (Table 1), while the high r_2/r_1 value indicates that the system is suitable for T_2-weighted MRI imaging. In case of cobalt ferrite nanoclusters the observed low relaxivities (r_1, r_2) can be attributed to the anisotropy of cobalt ferrite nanoparticles which are characterized as ferromagnetic particles and are not able to rotate their magnetization as fast as the manganese ferrite NPs under the specific experimental conditions. Moreover, the difference between

MnNCs and Mn@CoNCs stems from the different size of clusters (75 and 81 nm, respectively). Both clusters due to their size belong to the so-called motional average regime (MAR) where relaxivities increases in respect to the nanocluster diameter [46], as also indicated by us before [47].

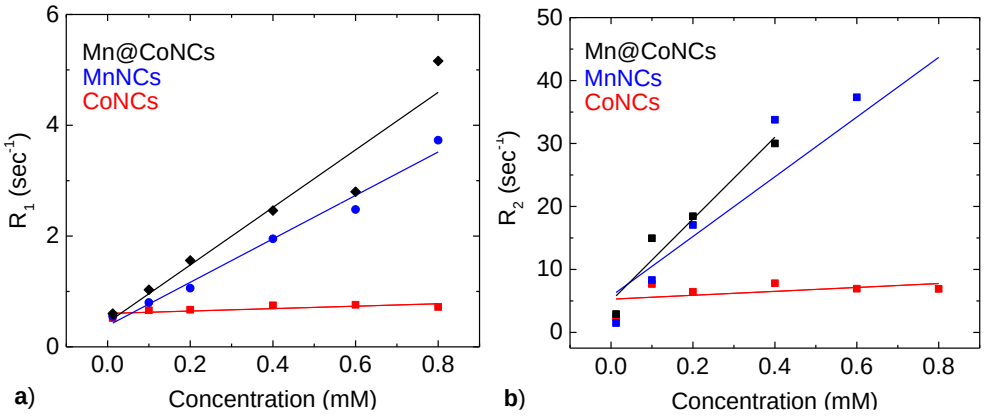

Fig. 6. (a) R_1 and (b) R_2 relaxation plots of aqueous suspensions of the three NCs samples as a function of concentration.

4. Conclusions

We have demonstrated a simple method for the formation of compact and spherical bi-magnetic nanoclusters (Mn@CoNCs) based on the microemulsion method. As building blocks manganese and cobalt ferrite nanoparticles of high crystallinity, low inversion degree and high Ms have been utilized based on our previous reports [30, 31]. In general, cobalt and manganese ferrite nanoparticles have already been proposed for biomedical purposes as they present optimal magnetic properties, while cytotoxicity studies showed that the low concentration and the sufficient surface coverage of the NPs permit their safe use as theranostic agents [48, 49]. For the clustering process we used the anionic surfactant SDS which is considered as a generally recognized as safe ingredient (GRAS) [50] and is used in several every day commercial products [51]

while can be find in a number of research work dealing with bioapplications [52, 53]. After the detection of the optimal SDS concentration well-defined NCs were formed with homogeneous distributed particles in their interior. Even though this hard/soft heterocomposite system does not present exchange coupling effects, the overall magnetic behavior reveals synergetic behavior as moderate coercivity and high magnetization values were obtained. The nanoclusters show a greatly improved response to external alternating magnetic fields, when compared to the constituent primary particles, resulting to high heat dissipation and strong contrast relaxivity, sustaining their multifunctional role and great potential as theranostic agents. In comparison with previously reported ferrite nanoclusters, the present magnetic systems present better heating performance [54-56], while their relaxivities are close to commercial products already used in clinical MRI (Feridex/Endorem) [57]. Moreover, this bi-magnetic ferrite system provides an excellent starting point for further theoretical and practical studies on nanomagnetism as coercivity could further be modulated by the proper selection of hard and soft magnetic volume fractions.

Acknowledgements

The authors would like to thank Assist. Prof. I. Tsougkos as well as Assist. Prof. K. Vasiou for their great assistance in MRI studies conducted at the University Hospital of Larissa.

References

[1] Z. Lu, Y. Yin, Colloidal nanoparticle clusters: functional materials by design, Chem. Soc. Rev. 41 (2012) 6874-6887.

[2] Y. Xia, Z. Tang, Monodisperse inorganic supraparticles: formation mechanism, properties and applications, Chem. Commun. 48 (2012) 6320-6336.

[3] T. Wang, D. LaMontagne, J. Lynch, J. Zhuang, Y. C. Cao, Colloidal superparticles from nanoparticle assembly, Chem. Soc. Rev. 42 (2013) 2804-2823.

[4] A. Kostopoulou, A. Lappas, Colloidal magnetic nanocrystal clusters: variable length-scale interaction mechanisms, synergetic functionalities and technological advantages, Nanotechnol. Rev. 4 (6) (2015) 595-624.

[5] E. S. G. Choo, X. Tang, Y. Sheng, B. Shuter, J. Xue, Controlled loading of superparamagnetic nanoparticles in fluorescent nanogels as effective T_2-weighted MRI contrast agents, J. Mater. Chem. 21 (2011) 2310-2319.

[6] C. Blanco-Andujar, D. Ortega, P. Southern, Q. A. Pankhurst, N. T. K. Thanh, High performance multi-core iron oxide nanoparticles for magnetic hyperthermia: microwave synthesis, and the role of core-to-core interactions, Nanoscale 7 (2015) 1768-1775.

[7] J. Ge, Y. Hu, M. Biasini, W. P. Beyermann, Y. Yin, Superparamagnetic magnetite colloidal nanocrystal clusters, Angew. Chem. Int. Ed. 46 (2007) 4342-4345.

[8] S. Xuan, F. Wang, Y. X. J. Wang, J. C. Yu, K. C. F. Leung, Facile synthesis of size-controllable monodispersed ferrite nanospheres, J. Mater. Chem. 20 (2010) 5086-5094.

[9] X. Hu, J. Gong, L. Zhang, J. C. Yu, Continuous Size Tuning of Monodisperse ZnO Colloidal Nanocrystal Clusters by a Microwave-Polyol Process and Their Application for Humidity Sensing, Adv. Mater. 20 (2008) 4845-4850.

[10] F. Bai, D. S. Wang, Z. Y. Huo, W. Chen, L. P. Liu, X. Liang, C. Chen, X. Wang, Q. Peng, Y. D. Li, A Versatile Bottom-up Assembly Approach to Colloidal Spheres from Nanocrystals, Angew. Chem. Int. Ed. 46 (2007) 6650-6653.

[11] D. E. Gomez, I. Pastoriza-Santos, P. Mulvaney, Tunable Whispering Gallery Mode Emission from Quantum-Dot-Doped Microspheres, Small 1 (2005) 238-241.

[12] Y. Lin, A. Böker, H. Skaff, D. Cookson, A. D. Dinsmore, T. Emrick, T. P. Russell, Nanoparticle Assembly at Fluid Interfaces: Structure and Dynamics, Langmuir 21 (2005) 191-194.

[13] J. Zhuang, H. Wu, Y. Yang, Y. C. Cao, Controlling Colloidal Superparticle Growth Through Solvophobic Interactions, Angew. Chem. Int. Ed. 47 (2008) 2208-2212.

[14] E. Peng, E. S. G. Choo, C. S. H. Tan, X. Tang, Y. Sheng, J. Xue, Multifunctional PEGylated nanoclusters for biomedical applications, Nanoscale 5 (2013) 5994-6005.

[15] Y. C. Chuang, C. J. Lin, S. F. Lo, J. L. Wang, S. C. Tzou, S. S. Yuan, Y. M. Wang, Dual functional AuNRs@MnMEIOs nanoclusters for magnetic resonance imaging and photothermal therapy, Biomaterials 35 (2014) 4678-4687.

[16] G. Zoppellaro, A. Kolokithas-Ntoukas, K. Polakova, J. Tucek, R. Zboril, G. Loudos, E. Fragogeorgi, C. Diwoky, K. Tomankova, K. Avgoustakis, D. Kouzoudis, A. Bakandritsos, Theranostics of Epitaxially Condensed Colloidal Nanocrystal Clusters, through a Soft Biomineralization Route, Chem. Mater. 26 (2014) 2062-2074.

[17] L. Lartigue, P. Hugounenq, D. Alloyeau, S. P. Clarke, M. Lévy, J.-C. Bacri, R. Bazzi, D. F. Brougham, C. Wilhelm, F. Gazeau, Cooperative Organization in Iron Oxide Multi-Core Nanoparticles Potentiates Their Efficiency as Heating Mediators and MRI Contrast Agents, ACS Nano 6 (2012) 10935-10949.

[18] S. H. Noh, W. Na, J. T. Jang, J. H. Lee, E. J. Lee, S. H. Moon, Y. Lim, J. S. Shin, J. Cheon, Nanoscale Magnetism Control via Surface and Exchange Anisotropy for Optimized Ferrimagnetic Hysteresis, Nano Lett. 12 (2012) 3716-3721.

[19] J. H. Lee, J. T. Jang, J. S. Choi, S. H. Moon, S. H. Noh, J. W. Kim, J. G. Kim, I. S. Kim, K. I. Park, J. Cheon, Exchange-coupled magnetic nanoparticles for efficient heat induction, Nat. Nanotechnol. 6 (2011) 418-422.

[20] Q. Song, Z. J. Zhang, Controlled synthesis and magnetic properties of bimagnetic spinel ferrite $CoFe_2O_4$ and $MnFe_2O_4$ nanocrystals with core-shell architecture, J. Am. Chem. Soc. 134 (2012) 10182-10190.

[21] Q. Zhang, I. Castellanos-Rubio, R. Munshi, I. Orue, B. Pelaz, K. I. Gries, W.J. Parak, P. Del Pino, A. Pralle, Model Driven Optimization of Magnetic Anisotropy of Exchange-Coupled Core–Shell Ferrite Nanoparticles for Maximal Hysteretic Loss, Chem. Mater. 27 (2015) 7380-7387.

[22] I. K. Schuller, S. Kim, C. Leighton, Magnetic superlattices and multilayers, J. Magn. Magn. Mater. 200 (1999) 571-582.

[23] G. Chern, L. Horng, W. K. Shieh, T. C. Wu, Antiparallel state, compensation point, and magnetic phase diagram of Fe_3O_4/Mn_3O_4 superlattices, Phys. Rev. B 63 (2001) 094421.

[24] A. Moser, A. Berger, D. T. Margulies, E. E. Fullerton, Magnetic tuning of biquadratic exchange coupling in magnetic thin films, Phys. Rev. Lett. 91 (2003) 097203.

[25] F. Liu, Y. Hou and S. Gao, Exchange-coupled Nanocomposites: Chemical Synthesis, Characterization and Applications, Chem. Soc. Rev. 43 (2014) 8098-8113.

[26] H. Zeng, J. Li, J. P. Liu, Z. L. Wang, S. Sun, Exchange-coupled nanocomposite magnets by nanoparticle self-assembly, Nature 420 (2002) 395-398.

[27] A. López-Ortega, M. Estrader, G. Salazar-Alvarez, A.G. Roca, J. Nogués, Applications of exchange coupled bi-magnetic hard/soft and soft/hard magnetic core/shell nanoparticles, Phys. Rep. 553 (2015) 1-32.

[28] E. E. Fullerton, J.S. Jiang, S.D. Bader, Hard/soft magnetic heterostructures: Model exchange-spring magnets, J. Magn. Magn. Mater. 200 (1999) 392-404.

[29] Z. Iatridi, K. Vamvakidis, I. Tsougos, K. Vasiou, C. Dendrinou-Samara, G. Bokias, A multifunctional polymeric platform of magnetic ferrite colloidal superparticles for luminescent, imaging and hyperthermia applications, ACS Appl. Mater. Interfaces 8 (2016) 35059-35070.

[30] K. Vamvakidis, M. Katsikini, D. Sakellari, E. C. Paloura, O. Kalogirou, C. Dendrinou-Samara, Reducing the inversion degree of $MnFe_2O_4$ nanoparticles through synthesis to enhance magnetization: evaluation of their ^1H NMR relaxation and heating efficiency, Dalton Trans. 43 (2014) 12754-12765.

[31] V. Georgiadou, C. Kokotidou, B. L. Droumaguet, B. Carbonnier, T. C. Papadopoulou, C. Dendrinou-Samara, Oleylamine as a beneficial agent for the synthesis of $CoFe_2O_4$ nanoparticles with potential biomedical uses, Dalton Trans. 43 (2014) 6377-6388.

[32] H. Mamiya, B. Jeyadevan, Optimal design of nanomagnets for targeted hyperthermia, J. Magn. Magn. Mater. 323 (2011) 1417-1422.

[33] K. Simeonidis, C. Martinez-Boubeta, L. Balcells, C. Monty, G. Stavropoulos, M. Mitrakas, A. Matsakidou, G. Vourlias, M. Angelakeris, Fe-based nanoparticles as tunable magnetic particle hyperthermia agents, J. Appl. Phys. 114 (2013) 103904-103908.

[34] T. Isojima, S. K. Suh, J. B. V. Sande, T. A. Hatton, Controlled Assembly of Nanoparticle Structures: Spherical and Toroidal Superlattices and Nanoparticle-Coated Polymeric Beads, Langmuir 25 (2009) 8292-8298.

[35] R. Klajn, K. J. M. Bishop, M. Fialkowski, M. Paszewski, C. J. Campbell, T. P. Gray, B. A. Grzybowski, Plastic and moldable metals by self-assembly of sticky nanoparticle aggregates, Science 316 (2007) 261-264.

[36] C. Ruiz, A photophysical study of the urea effect on micellar properties of sodium dodecylsulfate aqueous solutions, Colloid. Polym. Sci. 273 (1995) 1033-1040.

[37] C. P. Whitby, D. Fornasiero, J. Ralston, Effect of adding anionic surfactant on the stability of Pickering emulsions, J. Colloid and Inter. Sci. 329 (2009) 173-181.

[38] J. Chen, A. Dong, J. Cai, X. Ye, Y. Kang, J. M. Kikkawa, C. B. Murray, Collective dipolar interactions in self-assembled magnetic binary nanocrystal superlattice membranes, Nano Lett. 10 (2010) 5103-5108.

[39] M. Pauly, B. P. Pichon, P. Panissod, S. Fleutot, P. Rodriguez, M. Drillon, S. Begin-Colin, Size dependent dipolar interactions in iron oxide nanoparticle monolayer and multilayer Langmuir–Blodgett films, J. Mater. Chem. 22 (2012) 6343-6350.

[40] M.A. Radmanesh, S.A. Seyyed Ebrahimi, A. Yourdkhani , H. Khanmohammadi, Investigation of Magnetic Interactions in Core/Shell Structured $SrFe_{12}O_{19}/NiZnFe_2O_4$ Nanocomposite, J. Supercond. Nov. Magn. 25 (2012) 2757-2762.

[41] G. Muscas, P. Anil Kumar, G. Barucca, G. Concas, G. Varvaro, R. Mathieu, D. Peddis, Designing new ferrite/manganite nanocomposites, Nanoscale 8 (2016) 2081-2089.

[42] D. Maity, P. Chandrasekharan, P. Pradhan, K. H. Chuang, J. M. Xue, S. S. Feng, J. Ding, Novel synthesis of superparamagnetic magnetite nanoclusters for biomedical applications, J. Mater. Chem. 21 (2011) 14717-14724.

[43] B. Kozissnik, A. C. Bohorquez, J. Dobson, C. Rinaldi, Magnetic fluid hyperthermia: Advances, challenges, and opportunity, 972 Int. J. Hyperthermia 29 (2013) 706−714.

[44] S. Laurent, D. Forge, M. Port, A. Roch, C. Robic, L. Vander Elst, R. N. Muller, Magnetic Iron Oxide Nanoparticles: Synthesis, Stabilization, Vectorization,

Physicochemical Characterizations, and Biological Applications, Chem. Rev. 108 (2008) 2064−2110.

[45] R. A. Brooks, F. Moiny, P. Gillis, On T_2-shortening by weakly magnetized particles: the chemical exchange model, Magn. Reson. Med. 45 (2001) 1014-1020.

[46] Q. L. Vuong, P. Gillis, Y. Gossuin, Monte Carlo simulation and theory of proton NMR transverse relaxation induced by aggregation of magnetic particles used as MRI contrast agents, J. Magn. Reson. 44 (2011) 139–148.

[47] M. Menelaou, Z. Iatridi, I. Tsougos, K. Vasiou, C. Dendrinou-Samara G. Bokias, Magnetic colloidal superparticles of Co, Mn and Ni ferrite featured with comb-type and/or linear amphiphilic polyelectrolytes; NMR and MRI relaxometry, Dalton Trans. 44 (2015) 10980-10990.

[48] L. Wu, A. Mendoza-Garcia, Q. Li, S. Sun, Organic Phase Syntheses of Magnetic Nanoparticles and Their Applications, Chem. Rev. 116 (2016) 10473−10512.

[49] Z. Gao, T. Ma, E. Zhao, D. Docter, W. Yang, Roland H. Stauber, M. Gao, Small is Smarter: Nano MRI Contrast Agents – Advantages and Recent Achievements, Small 12 (2016) 556–576.

[50] 21 CFR 172.822 - Sodium lauryl sulfate gpo.gov. (2016).

[51] W. F. Bergfeld, Final report on the safety assessment of sodium lauryl sulfate and ammonium lauryl sulfate, Int. J. Toxicol. 24 (2016) 1-102.

[52] F. Pan, Z. Lu, I. Tucker, S. Hosking, J. Petkov, J. R. Lu, Surface active complexes formed between keratin polypeptides and ionic surfactants, JCIS 484 (2016) 125-134.

[53] L. Ye, W. E. Allen, K. R. Thompson, Q. Tian, B. Hsueh, C. Ramakrishnan, A. C. Wang, J. H. Jennings, A. Adhikari, C. H. Halpern, I. B. Witten, A. L. Barth, L. Luo, J. A. McNab, K. Deisseroth, Wiring and Molecular Features of Prefrontal Ensembles Representing Distinct Experiences, Cell 165 (2016) 1776–1788.

[54] D. Maity,P. Chandrasekharan, P. Pradhan, K. Chuang, J. Xue, S. Feng, J. Ding, Novel synthesis of superparamagnetic magnetite nanoclusters for biomedical applications, J. Mater. Chem. 21 (2011) 14717–14724.

[55] J. Xie, C. Yan, Y. Zhang, N. Gu, Shape Evolution of "Multi-Branched" Mn-Zn Ferrite Nanostructures with High-Performance: A Transformation of Nanocrystals into Nanoclusters, Chem. Mater. 25 (2013) 3702–3709.

[56] C. Blanco-Andujar, D. Ortega, P. Southern, Q. A. Pankhurst, N. T. K. Thanh, High performance multi-core iron oxide nanoparticles for magnetic hyperthermia: microwave synthesis, and the role of core-to-core interactions, Nanoscale 7 (2015) 1768–1775.

[57] M. Rohrer, H. Bauer, J. Mintorovitch, M. Requardt and H.-J. Weinmann, Comparison of magnetic properties of MRI contrast media solutions at different magnetic field strengths, Invest. Radiol. 40 (2005) 715–724.